Article

JOURNAL OF COMPOSITE MATERIALS

Journal of Composite Materials
0(0) 1–12

DOI: 10.1177/0021998311401107
jcm.sagepub.com

SAGE

Phase behaviour, microstructure, and percolation of poly(ethylene glycol) filled by multiwalled carbon nanotubes and organophilic montmorillonite

N.I. Lebovka[1], E. A. Lysenkov[2], A.I. Goncharuk[1], Yu.P. Gomza[2], V.V. Klepko[2] and Yu.P. Boiko[1]

Abstract

This work studies phase behavior, microstructure and percolation of the poly(ethylene glycol) (PEG), filled by multiwalled carbon nanotubes (MWCNTs), organo-modified montmorillonite (OMMT), and their mixtures, using differential scanning calorimentry (DSC), X-ray diffraction (XRD), electrical conductivity, and analysis of microscopic images. The DSC and XRD data showed a noticeable decrease of PEG crystallinity with increase of nanofiller content. Filling of PEG by MWCNTs was accompanied by a percolation threshold at ≈ 0.1 wt%, and the estimated electrical conductivity exponent ($t = 1.77 \pm 0.07$) was typical for the random percolation networks. The similar threshold behavior, but with higher percolation threshold ≈ 0.5–1.0 wt%, was observed for PEG filled by OMMT. The observed effect of OMMT-enhanced dispersion of MWCNTS in PEG at a high level of loading by nanoparticles offers good prospects for simultaneous improvement of the electrical and mechanical properties of PEG-based composites.

Keywords

poly(ethylene glycol), multiwalled carbon nanotubes, organo-modified montmorillonite, crystallinity, percolation

Introduction

Composites based on polymer electrolytes based on poly(ethylene glycol) (PEG), polyethylene oxide (PEO), etc., filled by nanoparticles of anisotropic shape (e.g., clays or nanotubes (NTs)), are attractive as materials with improved ionic and thermal conductivity, electrical, optical, and mechanical properties.[1]

The combination of PEG with plate-like montmorillonite (MMT) or organo-modified montmorillonite (OMMT) (so-called, PEG/MMT hybrids) improves barrier,[2] mechanical, viscoelastic, and thermal[3–5] properties of polymeric films. Existence of strong interaction between PEG and MMT was demonstrated by many studies. PEG chains can penetrate inside the interlayer of MMT and OMMT galleries.[6–9] Moreover, PEG can be used as a modifier for preparation of organoclays.[10] The PEG/MMT hybrids were shown to be useful for improving the rheological and mechanical properties of polypropylene,[10] polylactide[11], and rubber.[12]

The combination of PEG with rod-like NTs allows improvement of NT dispersion stability in common solvents.[13] Functionalization of carbon NTs[14] by, so-called, PEGylation, increases their solubility in water and aqueous solutions.[15] PEG-grafted multi-walled carbon NTs (PEG-g-MWCNTs) exhibited excellent hydrophilicity, good bioelectrocatalytic activity, and biocompatibility.[16] PEG functionalization enhances potential usefulness of such materials for biological systems and opens new prospects for future biomedical applications of NTs.[17] The chemical vapor and highly

[1]F. Ovcharenko Institute of Biocolloidal Chemistry, NAS of Ukraine, 42 Vernadskii Prosp., Kyiv 03142, Ukraine.
[2]Institute of Macromolecular Chemistry NAS of Ukraine 48, Kharkivske Shause, Kyiv 02160, Ukraine.

Corresponding author:
N.I. Lebovka, F. Ovcharenko Institute of Biocolloidal Chemistry, NAS of Ukraine, 42 Vernadskii Prosp., Kyiv 03142, Ukraine
Email: lebovka@gmail.com

selectivity gas sensors,[18,19] taste and bio-nanosensors[20,21] with fast response, good reproducibility, and high selectivity, which are based on PEG-functionalized carbon NTs, were already developed. Recently, PEO/multiwalled carbon nanotube (MWCNT) composites had attracted attention as potential materials for protection of optical sensors from high-intensity beams.[22]

The combination of polymers with mixture of MMT (OMMT) and MWCNTs (so-called, clay-supported carbon NTs) also attracted great interest.[23–25] This is a new class of materials with improved electrical and mechanical properties[26,27] which can find many interesting spheres of application, including sensors and biosensors, flame retardants, electromagnetic screens, reinforcements, gas barriers, ion batteries.[28,29] However, functionality of such multi-composites depends on compatibility of nanofiller components in the polymeric matrix, aggregation of nanoparticles, ability of reinforcement or conductive networking formation and its stability.[30] The presence of MMT significantly enhanced the state of dispersion of the carbon NTs in different media.[29–32] Obvious synergistic effects of MMT sheets and MWNT rods improving mechanical properties of polymeric composites were recently observed.[33–35] However, phase behavior and percolation effects in polymer electrolytes, filled by organic and inorganic fillers or their mixtures, are still far from full understanding and require more thorough studies.

This study discusses phase behavior, microstructure, and percolation effects in PEG-1000, filled by MWCNTs, OMMT, or their mixtures, studied by different experimental methods (differential scanning calorimentry (DSC), X-ray diffraction (XRD), electrical conductivity, and analysis of microscopic images).

Materials and methods

Samples

Poly-ethylene glycol (PEG-1000). PEG-1000 (M_w = 950–1050 g/mol) was an Aldrich product and chosen as representative polymer with high crystallinity degree. Before preparation of a composite, it was dewatered by heating in vacuum (2 mm) at residual pressure $p = 270$ Pa and temperature $T = 263$ K during 5 h. Its melting point determined from differential scanning calorimetric measurements was 308.0 K.

Multiwalled carbon nanotubes. The MWCNTs were prepared from ethylene by the method of chemical vapor deposition (SpecMash Ltd., Ukraine, fax: +380 44 5010620).[36] The residual mass content of the mineral additives was 0.1%. The specific surface area S of the MWCNTs, determined by adsorption of N_2, was about 130 m^2/g. Typically, such MWCNTs had mean outer diameter $d = 20$ nm, while their length l ranged from 5 to 10 μm. The specific electric conductivity σ of the powder of MWCNTs compressed at 15 TPa was about 10 S/cm along the axis of compression.

Montmorillonite, organo-modified montmorillonite and hybryde h(MWCNTs + OMMT). The pristine MMT was the MMT of Pygevskii deposit (Ukraine). The crude mineral was preliminary refined from impurities. For facilitation of MMT transfer into organic form, it was initially transferred into the sodium form through its multiple (five times) treatment by 0.1 molar solution of NaCl during 24 h at 340 K. The solid/liquid ratio was kept as 1/100. Then, MMT was centrifuged and washed several times by deionized water to remove surplus NaCl salt. The prepared sample of homoionic clay contained highly pure MMT, which was confirmed by X-ray and chemical analysis, and had the exchange capacity of 1.05 μmole-equ/g and the specific surface (determined by methylene blue adsorption) 640 m^2/g.

The OMMT was prepared by ion-exchange reactions. The long chain cetyl-trimethyl ammonium bromide ions ($C_{16}H_{33}N(CH_3)_3^+ \cdot Br^-$, CTAB, Merck) were chosen as a swelling agent for intercalation into MMT platelets, because they were shown to favor formation of exfoliated composites.[37–39] The aqueous solution of CTAB (1 wt%) was slowly added to the aqueous MMT dispersion (1 wt%) and stirred vigorously 24 h at 360 K. The quantity of solutions corresponded to the required 1:1 stoichiometric ratio of the exchange capacity of clay and CTAB. After incubation, dispersion was filtered using disc filter funnel and centrifuged. Finally, the obtained organomontmorillonite was freeze-dried for preserving its high dispersion ability in organic media.

The hybrid filler on the base of MWCNTs and OMMT was prepared by adding MWCNTs to the aqueous dispersion of MMT and CTAB during procedure of OMMT preparation. The ratio of MWCNTs to MMT was fixed at 1/10 by weight. Finally, the obtained hybrid filler was processed as OMMT filler.

Composite preparation. The composites were obtained by adding the appropriate weights of filler (MWCNTs, OMMT, or h(MWCNTs + OMMT) to PEG-1000 in the liquid state ($T = 323$ K) with subsequent 20 min sonication of the mixture using a UZDN-2T ultrasonic disperser, in accordance with procedure essentially similar to the previously described.[40]

After sonication, the composites were cooled down to the solid state and kept at room temperature until further experiments. We investigated a series of samples with content of NTs within 0.01–1 wt% and content of 0MMT within 0.01–1 wt%.

Characterization

Differential scanning calorimetry. DSC data, i.e., the phase transition temperatures and phase transition enthalpies, were measured with a TA Q2000 Instrument (TA Instruments Ltd. West Sussex, England) in the regime of heating from 273 to 333 K at the heating rate of 2 K/min. The samples (20–30 mg) were packed in the aluminium pans.

The fractional crystallinity of PEG-1000-based composites χ_{DSC} was calculated as:

$$\chi_{DSC} = \Delta H_m / \Delta H_m^o \quad (1)$$

where ΔH_m is the heat of melting of the composite under investigation and ΔH_m^o the heat of melting of 100% crystalline polymer (=165.5 J/g).[41,42] Though enthalpy method application for estimation of the crystallinity degree is controversial,[43] it is widely used for determination of the fractional crystallinity of PEGs,[44] and it is useful in applications with small filler content.

X-ray diffraction. The structure of composite at a small spatial scale was investigated using wide angle XRD instrument DRON-2 (Bourevestnik, Inc., St. Petersburg, Russia) with Cu-Kα source of emission at a wavelength $\lambda = 0.154$ nm.

The interlayer distance d of the MMT, OMMT, and h(MWCNTs + OMMT) was calculated from Bragg's formula:

$$\lambda = 2d \sin\theta \quad (2)$$

where θ is half of the diffraction angle and λ the wavelength.

The XRD patterns of MMT, OMMT, and h(MWCNTs + OMMT) are shown in Figure 1. The derived interlayer distance d is about 1.30 nm for montmorillonite, 1.90 nm for OMMT, and 2.0 nm for h(MWCNTs + OMMT).

The increase of interlayer distance d in organoclay OMMT evidenced that CTAB successfully penetrated into the MMT interlayer. Additional increase of d in hybrid h(MWCNTs + OMMT) filler, possibly, reflects strong interaction between MWCNTs and MMT. Existence of such interaction in aqueous suspensions was experimentally confirmed,[33] and it can be speculated that adsorption of MWCNTs on MMT can result in weakening of the inter-stack interactions and broadening of stacks.

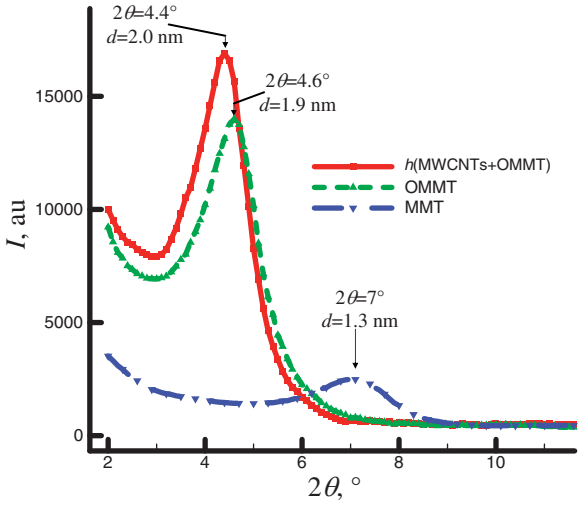

Figure 1. The XRD patterns of MMT, OMMT, and h(MWCNTs + OMMT).

The effective crystallite size L in the PEG-1000-based composites was estimated from Scherrer's equation, which can be used if the crystal is smaller than 100 nm[45]:

$$L = \alpha\lambda / \beta \cos\theta_m \quad (3)$$

where α is the coefficient accounting for the form of correlation zone (it is close to unity, $\alpha = 0.9$), β the width of a peak at half-height expressed in radians of 2θ (width measured in 2θ degrees and then multiplied by $\pi/180$), θ_m half of the diffraction angle corresponding to position of the scattering peak. For calculation of L, the most intensive maximum in the XRD pattern was used.

XRD patterns were used also for derivation of the fractional crystallinity of PEG-1000-based composites χ_{XRD} defined as a ratio:[46]

$$\chi_{XDR} = Q_c / Q_t \quad (4)$$

Here, Q_c is the part of area under the diffraction peak that corresponds to the crystalline structure and Q_t the total area under diffraction peak.

Electrical conductivity. The electrical conductivity σ was measured by the inductance, capacitance, and resistance (LCR) meter 819 Instek, 12 Hz–100 kHz (Instek America Corp. Chino, CA, USA) in a cell equipped with two horizontal platinum electrodes (diameter $d = 12$ mm, inter-electrode space $h = 0.5$ mm). The applied external voltage was $U = 1.275$ V. The measuring frequency of 10 kHz was chosen in order to avoid

polarization effects on the electrodes and the electric field-induced asymmetric redistribution of MWNTs between the electrodes.[47] The temperature T (287–363 K) was stabilized using a flowing-water thermostat of 100/45 type (Mechanik Pruefgeraete Medingen, Germany), and was recorded by a teflon-coated K type thermocouple (±0.1 K) connected to the data logger thermometer centre 309 (JDC Electronic SA, Switzerland). Preliminary studies have shown that nanoparticles aggregated irreversibly during the heating–cooling cycle in the temperature range corresponding to the liquid phase. So, a new sample was used in each experiment. The $\sigma(T)$ measurements were done in the temperature range of 280–365 K at the heating and cooling rate of $\approx$2 K/min.

Each measurement was repeated, at least, five times for calculation of the mean values of experimental data.

Microstructure. The optical microscopy images were obtained using an OI-3 UHL 4.2 microscope (LOMO, Russia). The microscope detector unit was interfaced with a digital camera and a personal computer.

The digital images were captured with magnification of 10–100, the layer thickness was 50 μm. In order to obtain 2D projections of the MWCNT aggregates, the focal plane was located, approximately, on the middle plane of the aggregates. The binary images were analyzed using the box-counting method with the help of the image analysis software ImageJ v1.42q. The 'capacity' fractal dimension d_f was obtained from dependence of the number of boxes necessary to cover the boundary of an aggregate N vs. the box size L:[48]

$$N \propto L^{d_f} \tag{5}$$

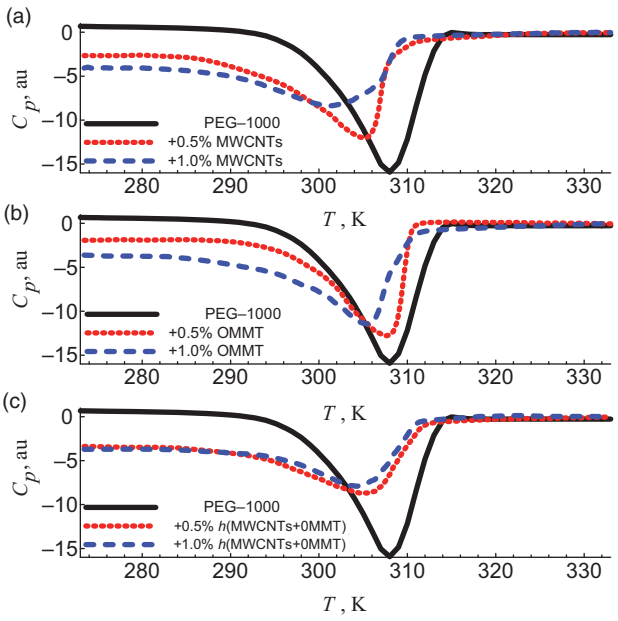

Figure 2. DSC endotherm traces for PEG-1000 filled by MWCNTs, OMMT, and h(MWCNTs + OMMT).

Table 1. DSC parameters of PEG-1000 filled by MWCNTs, OMMT, and h(MWCNTs + OMMT)

Sample	T_m (K) (±0.1)	ΔH_m (J/g) (±0.1)	χ_{DSC} (%) (±0.1)
PEG-1000	308.0	124.8	75.4
+0.5% MWCNTs	305.0	112.8	68.2
+1% MWCNTs	300.0	88.4	53.4
+0.5% OMMT	307.6	108.5	65.5
+1% OMMT	305.5	92.9	56.1
+0.5% h(MWCNTs + OMMT)	306.7	92.3	53.7
+1% h(MWCNTs + OMMT)	306.0	82.7	49.9

Results and discussion

Figure 2 presents a typical DSC endothermic traces of PEG-1000 filled by MWCNTs, OMMT, and h(MWCNTs + OMMT). Melting temperatures T_m taken as the melting peak maxima, T_m values, heats of melting ΔH_m, and fractional crystallinity χ_{DSC} are presented in Table 1. Introduction of nanofillers resulted in decrease of T_m, broadening of the melting peaks, decrease of ΔH_m and χ_{DSC}.

The value of χ_{DSC} decreased proportional to the percent of fillers replaced in the system. It evidences that the crystallinity of PEG was depressed next to the nanoparticle surface. It justifies the presence of specific interaction between PEG and surface of the investigated nanofiller. Such behavior even at a rather small concentration of nanofiller (0.5–1%) was expected because of the huge surface area of nanoparticles.

Figure 3 shows examples of the XRD patterns for the blank PEG-1000 and for PEG-1000 filled by MWCNTs, OMMT, and h(MWCNTs + OMMT).

The corresponding XRD parameters of composites are presented in Table 2. The introduction of nanoparticles in PEG-1000 resulted in decrease of XRD-derived fractional crystallinity and the estimated values of χ_{XRD} were in reasonable correspondence with χ_{DSC} estimations for the blank PEG-1000 and composites (Tables 1 and 2). Even at highest concentration of particles (=5%), the PEG-1000 displayed rather high degree of crystallinity in MWCNTs (χ_{XRD} = 51.3%) and OMMT-based (χ_{XRD} = 46.3–49.5%) nanofillers.

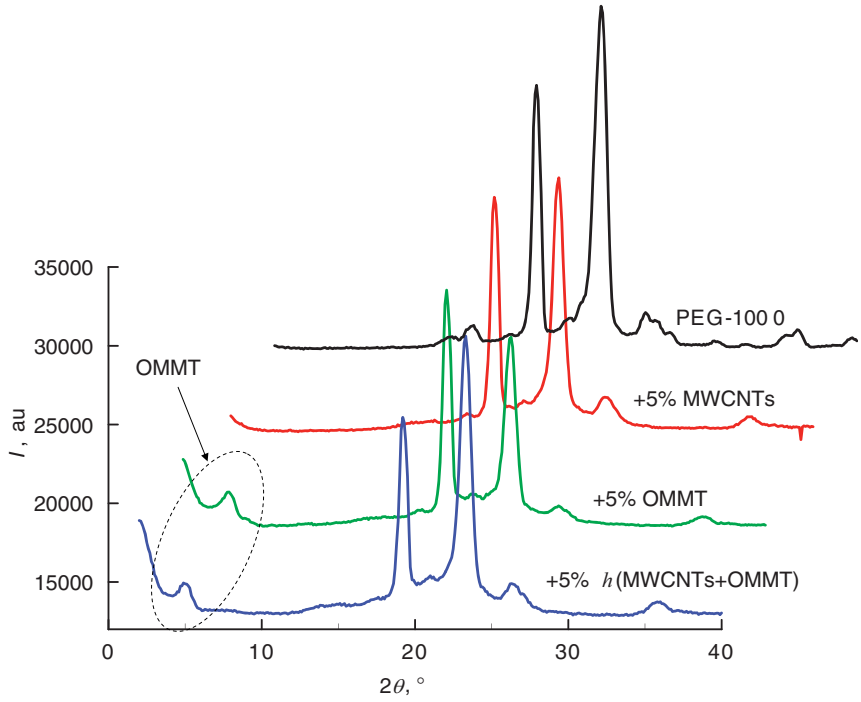

Figure 3. Examples of XRD patterns of PEG-1000 filled by MMT, OMMT, and h(MWCNTs + OMMT).

Table 2. XRD parameters for characterization of PEG-1000 filled by MWCNTs, OMMT, and h(MWCNTs + OMMT)

Sample	θ_m (°) ±0.1°	β (°) ±0.05°	L (nm) ±0.05 nm	χ_{XRD} (%) ±0.1%	θ_{OMMT} (°) ±0.05°	d (nm) ±0.05 nm
PEG-1000	23.3	0.75	11.80	78.3	–	–
+5% MWCNTs	23.4	0.70	13.85	51.2	–	–
+1% OMMT	23.3	0.90	10.00	52.0	4.75	1.85
+3% OMMT	23.3	0.75	11.55	49.8	4.85	1.80
+5% OMMT	23.3	0.75	12.55	46.3	5.00	1.75
+5% h(MWCNTs + OMMT)	23.2	0.65	12.90	49.5	5.00	1.75

For PEG-1000 filled by OMMT and h(MWCNTs + OMMT), the XRD patterns at ~5° contain the peaks corresponding to the OMMT stacks present in PEG-1000 (Figure 3). The derived interlayer distance d of the C_{OMMT} in PEG-1000 was a decreasing function of C_{OMMT} concentration (Table 2). It was the highest at $C_{OMMT} = 1\%$ ($d = 1.85$ nm); still, it was smaller than in CTAB-modified organoclay, $C_{OMMT} = 100\%$ ($d = 1.90$ nm). In principle, such behavior could be attributed to the partial substitution of CTAB modifier by PEG-1000 chains within the OMMT galleries and intercalation of polymer inside OMMT.[49] It was previously demonstrated that low molecular weight PEGs (PEG 200–PEG 4000) can effectively penetrate inside the interlayers of MMT and OMMT[6–8,50] and oxyethylene sequences of 5–6 units were proved to be sufficient for preparation of intercalated/exfoliated miscible PEG/MMT hybrids.[51]

It is worth mentioning that positions of the crystalline peaks in PEG-1000 practically did not change with introduction of the fillers (Table 2). However, their width was disturbed by the presence of nanoparticles. For highest concentration of filler (=5%), the crystallite size L was noticeably higher (12.55–13.85 nm) than in the blank PEG-1000 (11.8 nm).

The effect of nanofiller concentration on the crystalline structure of PEG composites is still unclear. The growth of the crystalline size, possibly, reflected the effects of orientational self-organization, and structure formation inside subsystems of nanoparticles with highly anisotropic shape.[52] Note that semi-crystalline structure of PEG reflects complex packing organization

of macromolecular PEG chains. PEG chains are arranged as helices at molecular level.[53] In the crystalline regions, these helices form lamellae that are, in turn, arranged into spherical units (spherulites).[54] The size of spherulites may be rather large (≈ 1.4 mm) at 302 K for PEG-2000.[55] The low molecular weight PEG chains are presumably extended or once-folded chains within the lamellae.[56]

Formation of lamellae can be disturbed by the surface of nanoparticles. That's why crystallization behavior and size of the crystallites can be quite different for PEG-based composites in comparison to other polymeric systems.[57] The nanoparticles can provide nucleation sites to polymer and accelerate the growth of spherulites.[58,59] It was shown that strong coordination of PEO to the MMT surface promotes non-crystalline PEO conformations, and crystallization of PEO was found to be inhibited.[60,61] Incorporation of MWCNTs reduced the crystallinity of PEO and restricted the spherical crystal growth and change of the crystal structure from spherical to disk like.[57] It was speculated that strong interactions and steric hindrance of PEG inside the networks formed by nanoparticles can disrupt the chain order and limit their possibility to move and rearrange.[60,61]

Examples of the electrical conductivity σ vs. temperature T dependencies of PEG-1000 filled by MWCNTs at different concentrations $C_{\mathrm{MWCNT}} = 0$–1% are presented in Figure 4. The electrical conductivity behavior of the blank PEG-1000 and it composites evidently reflects crystallization and melting processes. Blank PEG-1000 exhibited low ionic conductivity ($\sim 3 \times 10^{-7}$ S/cm) due to the presence of ionic impurities and an inherent proton generation process.[62] The ionic conductivity of PEG-1000 is strongly affected by the crystallinity of the material. In the blank PEG-1000, a clear melting-crystallization hysteretic loop was observed below the melting point ($T_{\mathrm{m}} = 308.0$ K). During the heating scan, the electrical conductivity σ noticeably increased in the vicinity of the melting point (from $\sigma = 3 \times 10^{-7}$ S/cm at $T = 398$ K to $\sigma = 2.6 \times 10^{-6}$ S/cm at $T = 310$ K). Such increase in conductivity of the blank PEG-1000 evidently reflects melting of the spherical structures (spherulites). It can be speculated that ionic conductivity enhancement near the melting point reflects rearrangements of helixes and hydroxyl end groups in the lamellae.[63] It is interesting that these rearrangements start in the solid phase at $T = 298$ K (i.e., below the melting point) and can reflect transformations between extended and once-folded (metastable) forms in PEG conformations.

For PEG-1000 + MWCNT composites, the melting-crystallization hysteretic loop (below 308.0 K) was similar to that observed for blank PEG-1000 at low concentration of NTs ($C_{\mathrm{MWCNT}} < 0.8\%$); however, it had a complex structure at higher concentration of NTs,

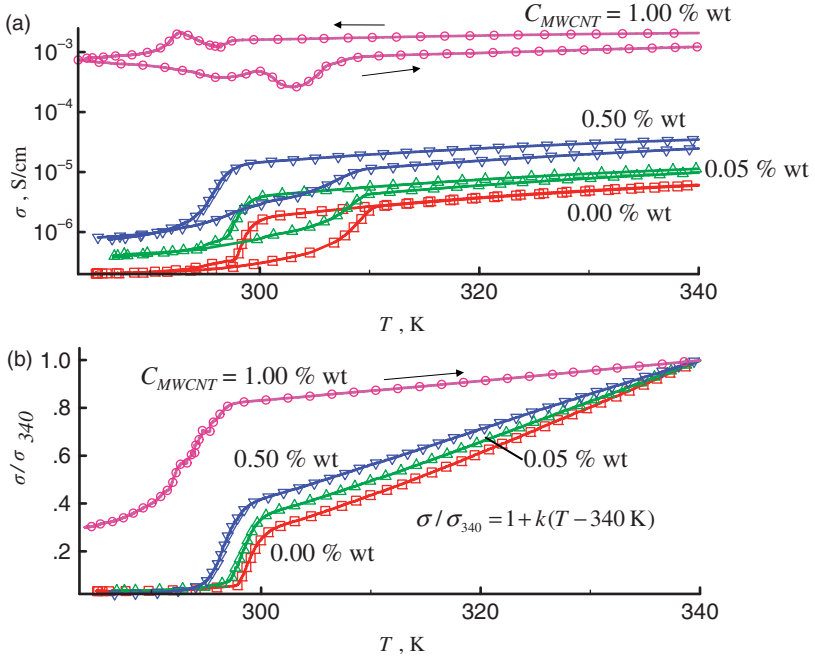

Figure 4. (a) Electrical conductivity σ vs. temperature T for PEG-1000 filled by MWCNTs at different concentrations $C_{\mathrm{MWCNT}} = 0$–1%. Arrows $\rightarrow$ and $\leftarrow$ correspond to the heating and cooling (2 K/min) cycles; (b) the same data are presented for cooling cycles as σ/σ_{340} vs. T, here $\sigma_{340} = \sigma(T = 340\ \mathrm{K})$.

$C_{MWCNT} = 1\%$ (Figure 4(a)). It can be explained by the effects of strong confinement of spherulites inside the network formed by MWCNTs.

Above the melting point T_m (>308 K), the electrical conductivity σ was an increasing function of temperature T and it displayed a very distinct hysteretic behavior in the heating–cooling cycles (Figure 4(a)). Such hysteretic behavior (thermal history effects) reflected the spatial rearrangement of MWNTs inside the PEG-1000 matrix during the heating–cooling cycles. The similar effects were previously reported for other fluidic composites filled by MWNTs.[64–66]

Typically, the electrical conductivity of polymeric systems above the melting point follows the non-Arrhenious behavior,[67] which can be approximated by the Vogel–Tammann–Fulcher (VTF) equation:

$$\sigma = \sigma_o \exp(-W/k(T - T_o)) \quad (6)$$

Here, σ_o is the pre-exponential factor that is proportional to the number of charge carriers in the system, kT the thermal energy, W the activation energy, and T_o the reference temperature roughly associated with the glass transition temperature T_g. T_o usually falls 25–60 K below T_g.

However, the experimental data have shown that for the PEG-1000 + MWCNT composites, the electrical conductivity σ in the temperature interval 300–340 K (cooling cycles) can be satisfactory fitted by the linear equation (Figure 4(b)):

$$\sigma = \sigma_{365}(1 + k(T - 340\ \mathrm{K})) \quad (7)$$

where σ_{340} is electrical conductivity at the fixed temperature $T = 340$ K and k the conductivity temperature coefficient.

Note that linear (non-Arrhenius) dependences are the typical for the conductivity governed by ionic mechanism. The conductivity temperature coefficient k was a decreasing function of C_{MWCNT} (Figure 5). This weakening of the temperature dependence of σ was in correspondence with the previously reported decreasing of the electrical conductivity activation energy in different composites loaded by MWNTs.[47,64,65] It was assumed that the observed behavior reflects the hopping junctions' mechanism of electrical transport between different MWNTs.[47] The elevation of temperature results in increase of the number of hopping junctions and in increase of electrical conductivity. Above the percolation threshold, the MWCNT networks become multiply connected and the temperature effects weaken.

The filling of PEG-1000 by MWCNTs was accompanied by a noticeable increase (by many orders of magnitude) in electrical conductivity σ. Such increase

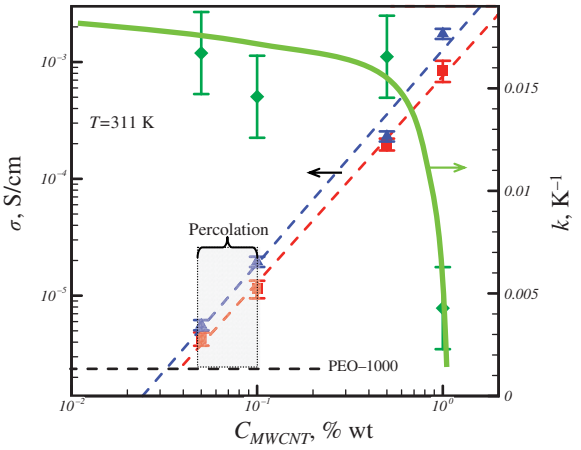

Figure 5. Electrical conductivity σ and conductivity temperature coefficient k vs. concentration C_{MWCNT} at $T = 311$ K in heating (■) and cooling (▲) cycles. $T = 311$ K.

of σ reflects formation of the percolating networks of MWCNTs. Typically, owing to the very large aspect ratio a (length to diameter ratio) of MWCNTs ($a = 500$–1000), the composites filled by MWCNTs demonstrated extremely low percolation thresholds C_c below 0.1–0.5 wt%.[64–68] For percolating systems with extremely low percolation threshold, the power law Archie's equation is fulfilled above the C_c:[49,69]

$$\sigma \propto C^t \quad (8)$$

where t is the conductivity exponent.

The least square fitting of experimental data by Equation (7) for PEG-1000 filled by MWCNTs gave $t = 1.77 \pm 0.07$ and correlation coefficient $\rho = 0.996$ (Figure 5). The value of conductivity exponent t was close to that typical for formation of random percolation networks.[69]

Figure 6(a) presents examples of the microscopic images of PEG-1000 composites with different concentrations of MWCNTs within 0.01–0.5% at $T = 310$ K (liquid phase). At small concentrations of MWCNTs ($C_{MWCNT} < 0.05\%$), the individual aggregates were observed (not shown); however, at $C_{MWCNT} = 0.1$ wt%, the aggregates were growing and connecting into a spanning percolation network (Figure 6(a)). It confirms the presence of the percolation threshold at $C_{MWCNT} = 0.1\%$ (Figure 4). The fractal dimension d_f was also estimated. It depicts morphology of the percolation aggregate in 2D projection (Figure 6(b)). Its value varies between 1 (corresponding to a linear aggregate) and 2 (corresponding to a compact aggregate). It was an increasing function of C_{MWCNT}, which is typical for behavior of the percolating MWCNT networks.[66]

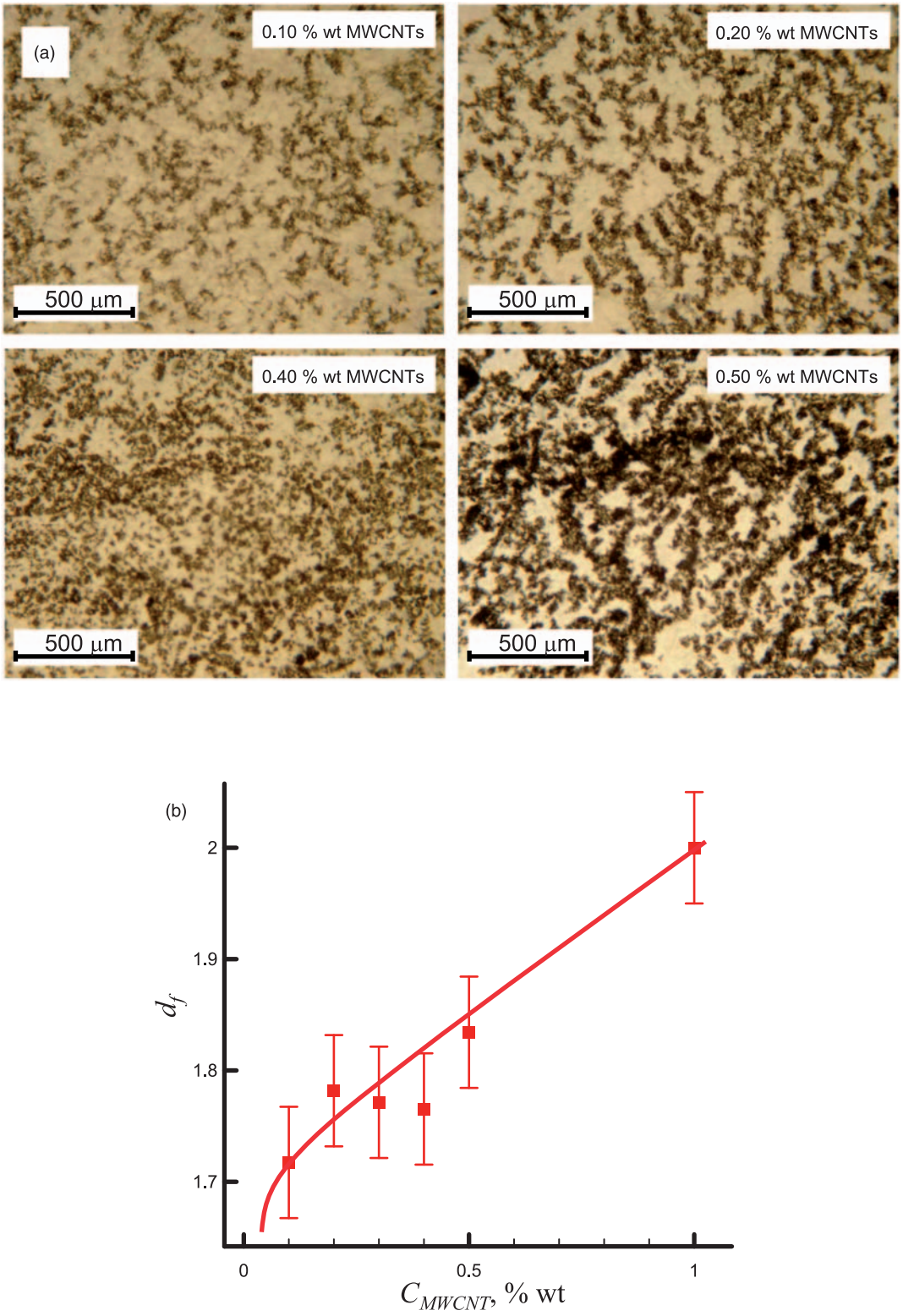

Figure 6. (a) Microscopic images of PEG-1000 filled by MWCNTs composites at different concentrations C_{MWCNT} wt%; (b) fractal dimension d_f vs. concentration of MWCNTs C_{MWCNT}. $T = 310$ K.

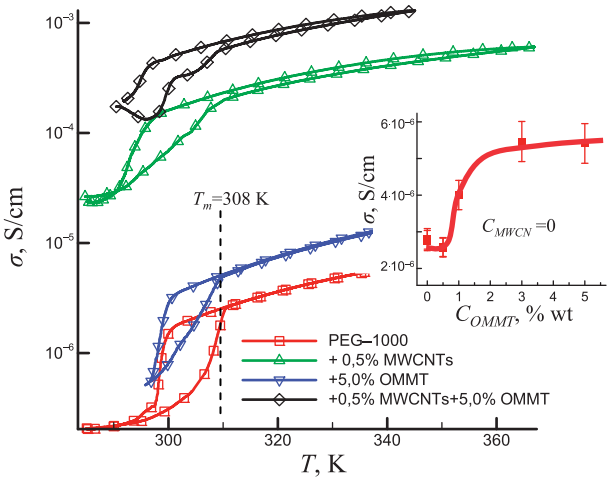

Figure 7. Electrical conductivity σ vs. temperature T for blank PEG-1000 and PEG-1000 filled by OMMT (5 wt%), MWCNTs (0.5%), and the mixture of OMMT (5 wt%) and MWCNTs (0.5%). Insert shows electrical conductivity σ vs. concentration of OMMT C_{OMMT} at $T = 310$ K.

Note that formation of percolation networks had no visible effect on behavior of the conductivity temperature coefficient k defined in Equation (7). It was approximately constant in a wide range of MWCNT concentrations ($C_{MWCNT} = 0$–0.5 wt%), and it decreased noticeably above C_{MWCNT} of 1 wt% (Figure 5). Such behavior reflected dominance of the ionic mechanism of conductivity through PEG-1000 conducting medium at $C_{MWCNT} = 0$–0.5 wt%.

However, direct and multiple contacts between individual NTs become important at high concentrations MWCNT. Weakening of the temperature dependence of σ is typical for MWCNT composites.[64–66,70,71]

Figure 7 demonstrates electrical conductivity σ vs. temperature T for PEG-1000 filled by MWCNTs, OMMT and mixture of MWCNTs and OMMT. The introduction of OMMT in PEG-1000 resulted in increase of the electrical conductivity σ (insert in Figure 6, $T = 310$ K). At small OMMT concentration ($C_{OMMT} < 0.5$ wt%), the effect OMMT on the total conductivity of the composite was rather small. The value of σ increased at higher concentrations of OMMT and reached saturation at large concentrations $C_{OMMT} > 2$–3 wt%. The observed effect resembles percolation transition for small electrical conductivity contrast (with percolation threshold between 0.5–1.0 wt%).

Increase of electrical conductivity σ with introduction of OMMT in PEG-1000 can be explained by exfoliation of OMMT, penetration of PEG-1000 inside the galleries of OMMT (intercalation), and partial substitution of ionic CTAB modifier by PEG-1000 chains. The presence of intercalation is evidenced by behavior of interlayer distance d of the OMMT (Table 2). Besides, it was previously demonstrated that clay intercalation and exfoliation may alter the ionic conductivity pathways in PEG/MMT hybrids.[7]

At high concentration of plate-like clay particles, $C_{OMMT} > 2.0$ wt%, the isotropic – nematic Onsager transition in a system of platelets is expected,[52] and at higher concentration of nanoplates, they start to form percolation networks. This process can restrict further exfoliation of OMMT galleries and increase of electrical conductivity σ with increase of C_{OMMT}. It can be speculated that the ionic transport is facilitated near the surface of OMMT platelets and this effect is the most pronounced for OMMT concentration above the percolation threshold.

The concentration of MWCNTs was noticeably above the percolation threshold ($C_{MWCNT} = 0.1$%). In the absence of OMMT, the MWCNTs formed obvious spanning networks (Figure 8) and the value of σ of the composite was two order of magnitude high than that of the blank PEG-1000. Addition of OMMT (0–5 wt%) to this composition (PEG-1000 + MWCNTs (0.5 wt%)) resulted in noticeable increase of σ (Figure 7). The microscopic images evidenced that addition of OMMT remarkably improved dispersion of MWCNTs inside the PEG-1000 matrix (Figure 8). The observed effects were in correspondence with the previously reported data on possibility of reduction of the percolation threshold in SWNT + epoxy composites by addition of clays.[35] The noticeable improvement of conductivity was observed above the percolation threshold and at high loadings by both MWCNTs (=0.5 wt%) and OMMT (5 wt%). Such high loadings offer good prospects for simultaneous improvement of electrical conductivity and mechanical properties of PEG-based composites.

Conclusions

Filling of PEG-1000 by nanoparticles (MWCNTs, OMMT, or their mixture) results in remarkable decrease of PEG crystallinity (up to ≈46–51%) and increase of the PEG crystallite size. It can be explained by strong interactions between PEG chains and surface of the nanoparticles. Filling of PEG-1000 by MWCNTs was accompanied by a noticeable increase (by two orders of magnitude) in electrical conductivity σ at the percolation threshold ≈0.1 wt%. The estimated electrical conductivity exponent was $t = 1.77 \pm 0.07$, which is typical for random percolation networks. The similar threshold behavior, but with smaller contrast and higher percolation threshold ≈0.5–1.0 wt%, was observed for PEG-1000 filled by OMMT. It was observed that additives of organoclay (OMMT) noticeably enhance dispersion of MWCNTs in PEG-1000 and

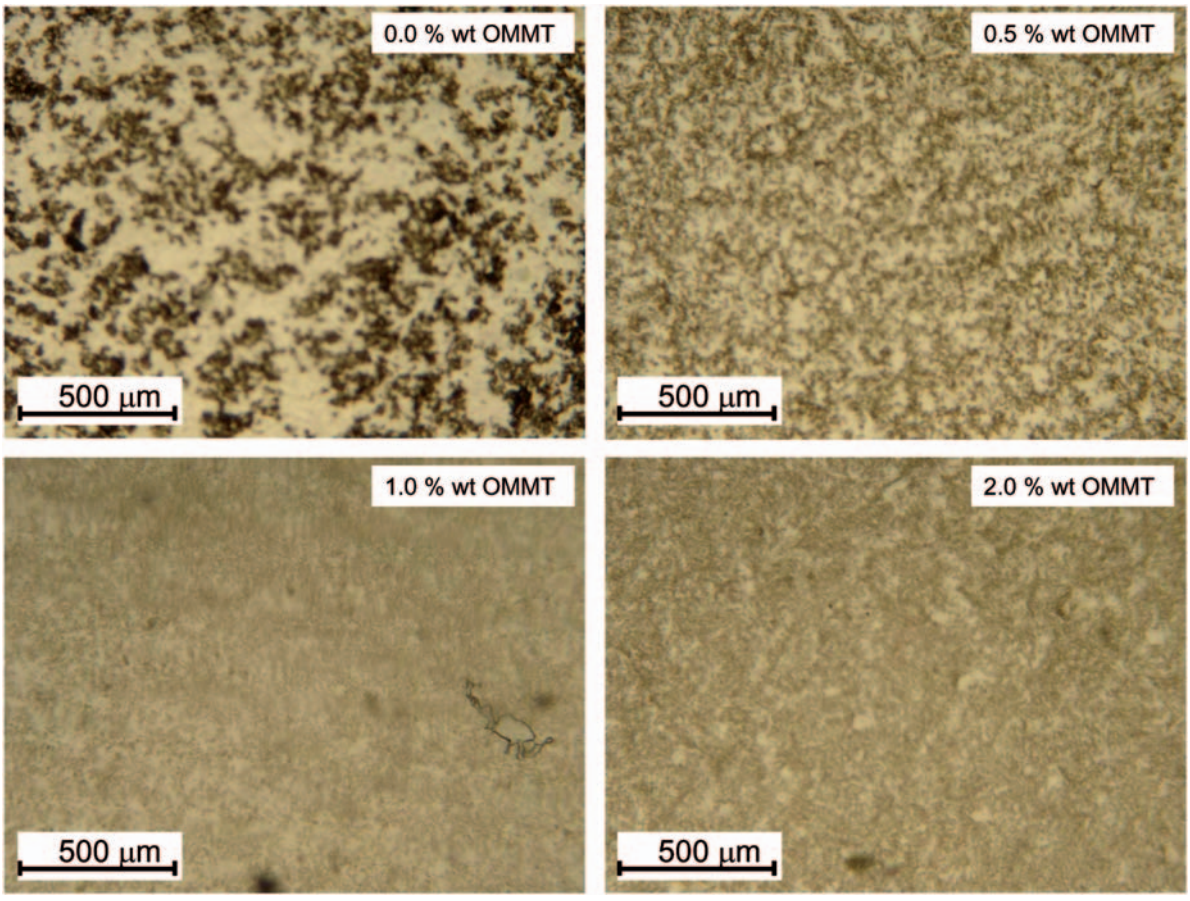

Figure 8. Microscopic images of PEG-1000 filled by MWCNTs ($C_{MWCNT} = 0.5$ wt%) and OMMT ($C_{OMMT} = 0$–2 wt%).

increase electrical conductivity of composite. Strong interactions between organic (MWCNTs) and inorganic (OMMT) nanoparticles were observed even at high level of nanoparticle loading, which offers good prospects for simultaneous improvement of electrical conductivity and mechanical properties of PEG-based composites.

Acknowledgments

This study was partially funded by the NAS of Ukraine under Projects 2.16.1.4, 2.16.1.7, and the Fund of Fundamental Studies F28.2/058. The authors thank Dr N.S. Pivovarova for her help with the manuscript preparation and Dr O.V. Melezhyk for providing the samples of MWCNTs.

References

1. Stefanescu EA, Daranga C and Stefanescu C. Insight into the broad field of polymer nanocomposites: from carbon nanotubes to clay nanoplatelets, via metal nanoparticles materials. *Materials* 2009; 2: 2095–2153.
2. Zenkiewicz M, Richert J and Rózański A. Effect of blow moulding ratio on barrier properties of polylactide nanocomposite films. *Polym Test* 2010; 29(2): 251–257.
3. Mohaddespour A, Abolghasemi H and Ahmadi SJ. The effect of nanoscaled-layered silicates on thermal conductivity of nanocomposites based on HDPE and PP. *J Compos Mater* 2008; 42(20): 2163–2174.
4. Lei HF, Wang P, Zhang YM and Yuan WB. Preparation and properties of plasticized poly(lactic acid) nano-composite with modified organo-montmorillonites. *Mater Sci Technol* 2009; 17(4): 457–461.
5. Ozkoc G and Kemaloglu S. Morphology, biodegradability, mechanical, and thermal properties of nanocomposite films based on PLA and plasticized PLA. *J Appl Polym Sci* 2009; 114(4): 2481–2487.
6. Chen B and Evans JRG. Preferential intercalation in polymer-clay nanocomposites. *J Phys Chem B* 2004; 108(39): 14986–14990.
7. Sengwa RJ, Choudhary S and Sankhla C. Dielectric spectroscopy of hydrophilic polymers–montmorillonite clay nanocomposite aqueous colloidal suspension. *Colloids Surf A* 2009; 336(1–3): 79–87.
8. Zampori L, Stampino PG, Cristiani C, Dotelli G and Cazzola P. Synthesis of organoclays using non-ionic surfactants: effect of time, temperature and concentration. *Appl Clay Sci* 2010; 48(1–2): 97–102.

9. Paul MA, Alexandre M, Degée P, Henrist C, Rulmont A and Dubois P. New nanocomposite materials based on plasticized poly(L-lactide) and organo-modified montmorillonites: thermal and morphological study. *Polymer* 2003; 44(2): 443–450.
10. Zhu S, Chen J and Li H. Influence of poly(ethylene glycol)/montmorillonite hybrids on the rheological behaviors and mechanical properties of polypropylene. *Polym Bull* 2009; 63(2): 245–257.
11. Lan J, Chen JY, Cao Y and Li HL. The mechanical properties and rheological behaviors of polylactide/montmorillonite nanocomposites. *Polym Mater Sci Eng* 2009; 25(7): 87–89.
12. Carretero-González J, Valentín JL, Arroyo M, Saalwächter K and Lopez-Manchado MA. Natural rubber/clay nanocomposites: influence of poly(ethylene glycol) on the silicate dispersion and local chain order of rubber network. *Eur Polym J* 2008; 44(11): 3493–3500.
13. Amiran J, Nicolosi V, Bergin SD, Khan U, Lyons PE and Coleman JN. High quality dispersions of functionalized single walled nanotubes at high concentration. *J Phys Chem C* 2008; 112(10): 3519–3524.
14. Kubota S, Maruyama T, Nishikiori H, Tanaka N, Endo M and Fujii T. Spectroscopic evaluation of the length of poly(ethylene glycol) covalently attached to multiwalled carbon nanotubes. *Chem Lett* 2009; 38(9): 890–891.
15. Chattopadhyay J, De Jesus Cortez F, Chakraborty S, Slater NKH and Billups WE. Synthesis of water-soluble PEGylated single-walled carbon nanotubes. *Chem Mater* 2006; 18(25): 5864–5868.
16. Wen Y, Wu H, Chen S, Lu Y, Shen H and Jia N. Direct electrochemistry and electrocatalysis of hemoglobin immobilized in poly(ethylene glycol) grafted multiwalled carbon nanotubes. *Electrochim Acta* 2009; 54(27): 7078–7084.
17. Liu Z, Davis C, Cai W, He L, Chen X and Dai H. Circulation and long-term fate of functionalized, biocompatible single-walled carbon nanotubes in mice probed by Raman spectroscopy. *Proc Natl Acad Sci USA* 2008; 105(5): 1410–1415.
18. Lee J, Park EJ, Choi J, Hong J and Shim SE. Polyurethane/PEG-modified MWCNT composite film for the chemical vapor sensor application. *Synth Met* 2010; 160(7–8): 566–574.
19. Niu L, Luo Y and Li Z. A highly selective chemical gas sensor based on functionalization of multi-walled carbon nanotubes with poly(ethylene glycol). *Sens Actuators B* 2007; 126(2): 361–367.
20. Hirata T, Amiya S, Akiya M, Takei O, Sakai T, Nakamura T, et al. Chemical modification of carbon nanotube based bio-nanosensor by plasma activation. *Jpn J Appl Phys* 2008; 47: 2068–2071.
21. Takagi K, Hirata T and Akiya M. A taste sensor based on a carbon nanotubes. *IEEJ Trans Sens Micromach* 2009; 129(10): 333–337.
22. Jin Z, Sun X, Xu G, Goh SH and Ji W. Nonlinear optical properties of some polymer/multi-walled carbon nanotube composites. *Chem Phys Lett* 2000; 318: 505–510.
23. Bakandritsos A, Simopoulos A and Petridis D. Carbon nanotube growth on a swellable clay matrix. *Chem Mater* 2005; 17: 3468–3474.
24. Zhang WD, Phang IY and Liu TX. Growth of carbon nanotubes on clay: unique nanostructured filler for high-performance polymer nanocomposites. *Adv Mater* 2006; 18: 73–77.
25. Feng J and Wang Q. Fabrication of nanocomposite powders of carbon nanotubes and montmorillonite. *J Am Ceramic Soc* 2008; 91(3): 975–978.
26. Mei QL, Wang JH, Xu S and Huang ZX. Rheology and curing characteristics of MWCNTs-OMMT epoxy composites. *Polym Mater Sci Eng* 2009; 25(6): 49–52.
27. Zhao YQ, Lau KT, Wang Z, Wang ZC, Cheung HY, Yang Z, et al. Fabrication and properties of clay-supported carbon nanotube/poly (vinyl alcohol) nanocomposites. *Polym Compos* 2009; 30(6): 702–707.
28. Gawryla MD, Liu L, Grunlan JC and Schiraldi DA. PH tailoring electrical and mechanical behavior of polymer-clay-nanotube aerogels. *Macromol Rapid Commun* 2009; 30(19): 1669–1673.
29. Lisunova MO, Lisunova YO, Le S, Kim J, Joo K and Zang D. The influence of organophilic clay on field electron emission uniformity and lifetime of screen printed carbon nanotube film. *Thin Solid Films* 2009; 518(1): 279–283.
30. Pack S, Kashiwagi T, Stemp D, Koo J, Si M, Sokolov JC, et al. Segregation of carbon nanotubes/organoclays rendering polymer blends self-extinguishing. *Macromolecules* 2009; 42(17): 6698–6709.
31. Han Z, Zhang F, Lin D and Xing B. Clay minerals affect the stability of surfactant-facilitated carbon nanotube suspensions. *Environ Sci Technol* 2008; 42(18): 6869–6875.
32. Lan YF and Lin JJ. Observation of carbon nanotube and clay micellelike microstructures with dual dispersion property. *J Phys Chem A* 2009; 113(30): 8654–8659.
33. Wang Z, Meng X, Li J, Du X, Li S, Jiang Z, et al. A simple method for preparing carbon nanotubes/clay hybrids in water. *J Phys Chem C* 2009; 113(19): 8058–8064.
34. Mei Q, Wang J and Huang Z. Synergistic effect of multiwall carbon nanotube and organophilic montmorillonite on toughening epoxy resin. *Acta Mater Compos Sin* 2008; 25(6): 146–151.
35. Liu L and Grunlan JC. Clay assisted dispersion of carbon nanotubes in conductive epoxy nanocomposites. *Adv Funct Mater* 2007; 17: 2343–2348.
36. Melezhyk AV, Sementsov YuI and Yanchenko VV. Synthesis of fine carbon nanotubes co-deposited at metallic oxide catalysts. *Appl Chem* 2005; 78: 938–943 (in Russian).
37. Alexandre M and Dubois P. Polymer-layered silicate nanocomposites: preparation, properties and uses of a new class of materials. *Mater Sci Eng* 2000; 28: 1–63.
38. Chashechnikova I, Dolgov L, Gavrilko T, Puchkovska G, Shaydyuk Ye, Lebovka N, et al. Optical properties of heterogeheous nanosystems based on montmorillonite clay mineral and 5CB nematic liquid crystal. *J Mol Struct* 2005; 563: 744–747.
39. Bezrodna T, Chashechnikova I, Dolgov L, Puchkovska G, Shaydyuk Ye, Lebovka N, et al. Effects of

montmorillonite modification on optical properties of heterogeneous nematic liquid crystal – clay mineral nanocomposites. *Liq Cryst* 2005; 32: 1005–1012.
40. Lisunova MO, Lebovka NI, Melezhyk OV and Boiko YuP. Stability of the aqueous suspensions of nanotubes in the presence of nonionic surfactant. *J Colloid Interface Sci* 2006; 299(2): 740–746.
41. Wieczorek W, Zalewska A, Raducha D, Florjańczyk Z and Stevens JR. Composite polyether electrolytes with lewis acid type additives. *J Phys Chem B* 1998; 102(2): 352–360.
42. Chen HW and Chang FC. The novel polymer electrolyte nanocomposite composed of poly(ethylene oxide), lithium triflate and mineral clay. *Polymer* 2001; 42(24): 9763–9769.
43. Kong Y and Hay JN. The enthalpy of fusion and degree of crystallinity of polymers as measured by DSC. *Eur Polym J* 2003; 39(8): 1721–1727.
44. Pielichowski K and Flejtuch K. Differential scanning calorimetry studies on poly(ethylene glycol) with different molecular weights for thermal energy storage materials. *Polym Adv Tech* 2002; 13(10–12): 690–696.
45. Guinier A. *Théorie et technique de la radiocristallographie*. Paris: Dunod, 1964.
46. Matthews JL, Peiser HS and Richards RB. The X-ray measurement of the amorphous content of polythene samples. *Acta Crystallogr* 1949; 2(1): 85–90.
47. Liu L, Yang Y and Zhang Y. A study on the electrical conductivity of multi-walled carbon nanotube aqueous solution. *Physica E* 2004; 24: 343–348.
48. Feder J. *Fractals*. New York: Plenum Press, 1988.
49. Archie GE. The electrical resistivity log as an aid in determining some reservoir characteristics. *Petrol Trans AIME* 1942; 146: 54–56.
50. Deng Y, Dixon JB and White GN. Bonding mechanisms and conformation of poly(ethylene oxide)-based surfactants in interlayer of smectite. *Colloid Polym Sci* 2006; 284(4): 347–356.
51. Lu Y, Kong ST, Deiseroth HJ and Mormann W. Structural requirements for the intercalation of polyether polyols into sodium-montmorillonite: the role of oxyethylene sequences. *Macromol Mater Eng* 2008; 293(11): 900–906.
52. Mourad MCD, Wijnhoven JEGJ, van Zand DD, van der Beek D and Lekkerkerker HNW. Gelation versus liquid crystal phase transitions in suspensions of plate-like particles. *Phil Trans Royal Soc A* 2006; 364(1847): 2807–2816.
53. Tadokoro H. Structures of crystalline polyethers. *Macromol Rev* 1966; 1: 119–172.
54. Craig DQM and Newton JM. Characterisation of polyethylene glycols using differential scanning calorimetry. *Int J Pharm* 1991; 74: 33–41.
55. Korotkikh NI, Matveev NN and Sidorkin AS. Pyroelectric properties of polyethylene oxide. *Phys Solid State* 2009; 51(6): 1290–1292.
56. Buckley CP and Kovacs AJ. Melting behaviour of low molecular weight poly(ethylene oxide) fractions, 2: folded chain crystals. *Coll Polym Sci* 1976; 254(1): 695–715.
57. Jin J, Song M and Pan F. A DSC study of effect of carbon nanotubes on crystallisation behaviour of behaviour of poly(ethylene oxide). *Thermochim Acta* 2007; 456: 25–31.
58. Haggenmueller R, Ficher JE and Winey KI. Single wall carbon nanotube/polyethylene nanocomposites: thermal and electrical conductivity. *Macromolecules* 2006; 39: 2964.
59. Probst O, Moore EM, Resasco DE and Grady BP. Nucleation of polyvinyl alcohol crystallization by single-walled carbon nanotubes. *Polymer* 2004; 45: 4437.
60. Strawhecker KE and Manias E. Crystallization behavior of PEO in the presence of Na+ montmorillonite fillers. *Chem Mater* 2003; 15: 844–849.
61. Stefanescu EA, Stefanescu C, Daly WH, Schmidt G and Negulescu II. Hybrid polymer–clay nanocomposites: a mechanical study on gels and multilayered films. *Polymer* 2008; 49: 3785–3794.
62. Gray FM. *Solid polymer electrolyte – fundamentals and technological applications*. New York: VCH Publishers, 1991.
63. Kovacs AJ, Gonthier A and Straupe C. Isothermal growth, thickening and melting of poly(ethylene oxide) single crystals in the bulk. *J Polym Sci* 1975; 50(1): 283–325.
64. Lebovka N, Dadakova T, Lysetskiy L, Melezhyk O, Puchkovska G, Gavrilko T, et al. Phase transitions, intermolecular interactions and electrical conductivity behavior in carbon multiwalled nanotubes/nematic liquid crystal composites. *J Mol Struct* 2008; 877(1–3): 135–143.
65. Lebovka NI, Goncharuk A, Melnyk VI and Puchkovska GA. Interface interactions in benzophenone doped by multiwalled carbon nanotubes. *Physica E* 2009; 41: 1554–1560.
66. Goncharuk AI, Lebovka NI, Lisetski LN and Minenko SS. Aggregation, percolation and phase transitions in nematic liquid crystal EBBA doped with carbon nanotubes. *J Phys D* 2009; 42: 165411.
67. Patel SK, Patel RB, Awadhia A, Chand N and Agrawal SL. Role of polyvinyl alcohol in the conductivity behaviour of polyethylene glycol-based composite gel electrolytes. *PRAMANA Indian Acad Sci* 2007; 69(3): 467–475.
68. Lisunova MO, Mamunya YeP, Lebovka NI and Melezhyk AV. Percolation behaviour of ultrahigh molecular weight polyethylene/multi-walled carbon nanotubes composites. *Eur Polym J* 2007; 43(3): 949–958.
69. Stauffer D and Aharony D. *Introduction to percolation theory*. London: Taylor & Francis, 1994.
70. Dolgov L, Kovalchuk O, Lebovka N, Tomylko S and Yaroshchuk O. Liquid crystal dispersions of carbon nanotubes: dielectric, electro-optical and structural peculiarities. In: *Carbon nanotubes*. Croatia: In-Tech Vukovar, 2010, pp.451–483.
71. Ponevchinsky VV, Goncharuk AI, Vasil'ev VI, Lebovka NI and Soskin MS. Cluster self-organization of nanotubes in a nematic phase: the percolation behavior and appearance of optical singularities. *JETP Lett* 2010; 91(5): 241–244.